1st International Conference on 3D Materials Science
Edited by: Marc De Graef, Henning Friis Poulsen, Alexis Lewis, Jeff Simmons, George Spanos
TMS (The Minerals, Metals & Materials Society), 2012

3D Investigation of Cracking Behavior in a Ni Superalloy

Andrew Deal[1], David Rowenhorst[2], Brandon Laflen[1], Ian Spinelli[1],
Tony Barbuto[1], Yuchi Huang[1], Timothy Hanlon[1]

[1]GE Global Research; 1 Research Circle; Niskayuna, NY 12309
[2]The U.S. Naval Research Laboratory; 4555 Overlook Avenue SW, Washington, DC 20375

Abstract

The high temperature fatigue performance of Ni-base superalloys is critical to gas turbine applications and as such, requires a more fundamental understanding when designing and producing turbine components. To investigate the relationship to local microstructure, a fatigue specimen was cycled under conditions designed specifically to result in intergranular propagation. Prior to failure, the test was interrupted and a 3D data set was reconstructed destructively from optical and EBSD slices taken from around the tip of the growing crack. The data set was investigated to understand the character of grain boundary planes along the crack front with respect those of the bulk material.

Introduction

Gas turbines demand exceptional high temperature material performance. Standard operation imposes complex cyclic stress states and corrosive environments, making alloy design crucial to component life. Consequently, it is no misnomer that the class of alloys suited for gas turbine applications are called 'superalloys.' In service Ni superalloys must survive a number of engine cycles in the range of 15,000 or 150,000, depending on the application, and this expected life is currently set through curves generated by thorough mechanical testing. To supplement this data and understand the microstructural effects on life, an effort to explore the three-dimensional nature of a crack tip was initiated. Methodology and preliminary results are discussed here.

Mechanical Testing

A Ni-base superalloy fatigue specimen with rectangular cross section (0.400” wide by 0.168” thick), known as a KB bar, was prepared with a 7-mil deep by 14-mil wide EDM surface flaw in the center of the gage section. An image of a KB bar is shown in Figure 1. The specimen blank was fully solutioned and aged, prior to finish-machining. A room temperature pre-crack sequence was imposed at 10Hz under a constant ΔK of 14.25ksi*in$^{1/2}$ (R = 0.05) to extend a fatigue crack from the EDM starter flaw. The test temperature was then elevated to 1300°F and a trapezoidal cyclic waveform was imposed with 1-second ramps and a 360-second hold at peak stress. This combination of temperature, stress, and waveform resulted in a fully intergranular fatigue failure mode. Crack length measurements were made throughout with a reversing DC electrical potential drop system. The test was interrupted prior to failure, and the specimen was prepared for serial sectioning to analyze the microstructure adjacent to the main crack.

To prepare the sample, a section of the KB bar containing the fatigue crack was mounted in a conductive phenolic compound, ground, and polished in longitudinal cross-section. The grinding was controlled so that the plane of the final polish was approximately transversely centered in the bar, capturing the deepest part of the crack. Additionally, the cross-section was mounted

away from the mount center and a flat was polished into the side of the mount for positioning in the SEM and the optical bench.

Data Acquisition

Once the mount was prepared, a serial sectioning routine similar to [1] was applied to generate data for 3D reconstruction and analysis. First, four Knoop micro-indents were set in a rectangular array surrounding the crack tip using a Clemex JS-2000 micro-indenter. The initial width of each indent was measured and recorded to provide a baseline for measuring material removal. Next the mount was positioned in a Struer's Prepamatic-2 autopolisher and nominally 1.0μm of material was removed. A modified Kalling's etch was applied to delineated the grain boundaries and a multi-image optical montage of the entire crack tip was taken on a Zeiss Axio Observer Z1.m microscope, with a 0.11μm pixel size. The indent widths were measured again after the polish and imaging, and the removal depth was calculated using the geometry of the indent. This sequence was repeated five times, with fresh indents being applied every other slice in a rotating pattern. Once the fifth cycle was completed the flat of the sample was placed in a Camscan 44 W-filament SEM on a 20° pre-tilted wedge with affixed stoppers for accurate sample positioning. This positioning provided a 70° tilt of the sample plane for EBSD mapping. Once the SEM was evacuated, the accelerating voltage was set to 20kV and sample was positioned to map the region of interest. Before scanning, the filament was allowed to equilibrate for a minimum of 3 hours in order to minimize drift during mapping. Finally a 1631x1259 pixel map, with a step size of 0.75 μm, was performed. The map took approximately 13 hours to complete at a scan rate of 44 points/second. The entire sub-process of 5 optical analyses and one EBSD analysis was repeated over the course of 4 months to produce ~150 individual optical slices and ~30 EBSD maps for the 3D reconstruction, schematically shown in Figure 1.

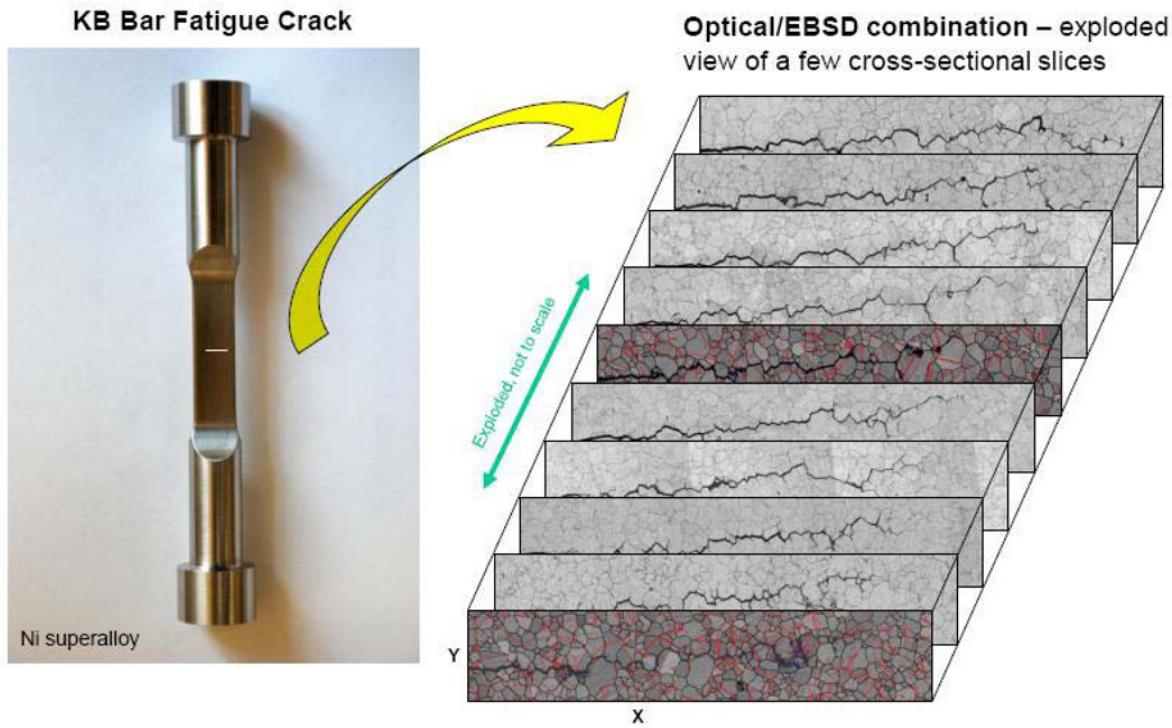

Figure 1 – Schematic representation of KB bar crack 3D reconstruction

Results

Figure 2 shows the removal rate histogram for the 150 slices. The standard deviation of the mechanical material removal was 0.21µm, and the overall average was 1.01µm, within 1% of the target. A typical optical montage and a corresponding EBSD map are shown in Figure 3. The optical montages generally did not reveal twin boundaries. Some are visible, but most are not. However, twins were well captured by the EBSD maps, which will eventually allow for their incorporation into the reconstruction. The percentage of correctly indexing points in the EBSD maps was generally 95% or more. Cleanup was applied to the data to fill in grain boundaries, but care was taken to avoid filling the crack to aid in crack extraction. In Figure 3, ~3.5% of points were generated from the cleanup routine, with red indicating a Σ3 boundary, black indicating a regular grain boundary, green representing the remaining unindexed area.

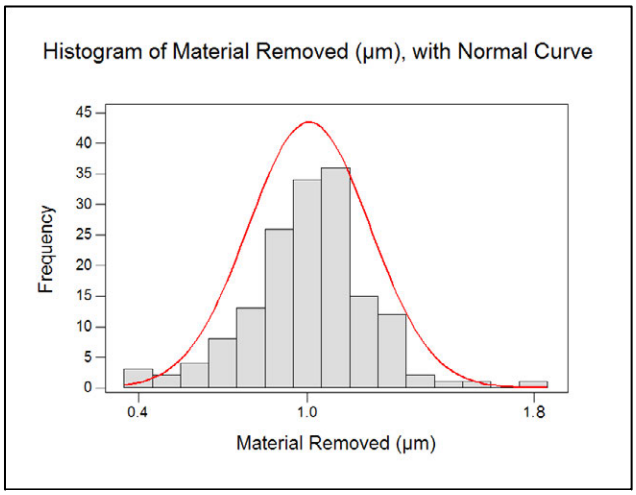

Figure 2 – Histogram of sectioning measurements

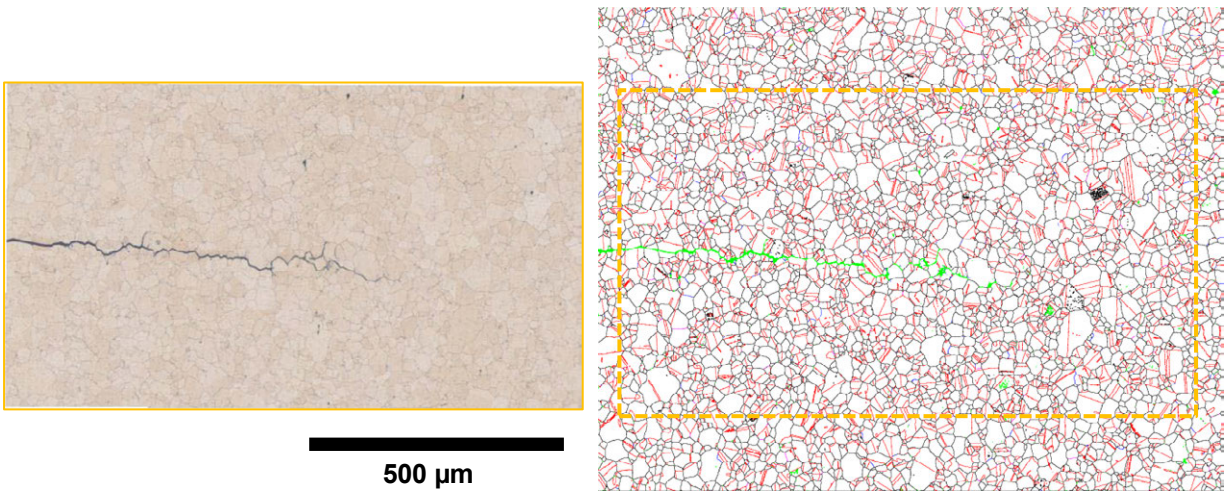

Figure 3 – Typical optical montage (L) and EBSD map (R). Black, red, and green in the map signify regular boundaries, special boundaries, and unindexed points, respectively.

Data Reconstruction

To reconstruct the 3D volume, first the individual optical tiles from each slice were montaged using the Zeiss software. The optical images were then stacked and aligned within the computer using in-house registration routines. The misalignments between the sections primarily consisted of translations, with very small rotational misalignments. The translations were determined by the maximum in the cross-correlation of the images.

Next the EBSD scans were aligned with the optical images. While the task of matching two images of the same identical area might seem easier than aligning different sections, the alignment of the two image modalities proved to be more challenging. One difficulty was that the EBSD images had small inherent distortions. These distortions were likely due to small amounts of drift, minor errors in dynamic focus or electron beam raster alignment to the sample, and some small sample positional errors. For more information on distortions in EBSD maps, see [2]. While careful data collection methods minimized these distortions, when directly comparing small features over a large area, such as the interface of a crack, even small image distortions led to significant misalignment of the images.

To align the two datasets, the optical image was treated as the baseline image, and its sister EBSD image was undistorted to achieve the highest degree of overlap with it. The EBSD image was undistorted using a second-degree polynomial with separate coefficients for the x and y directions, leading to a 12 parameter optimization. The coefficients of the polynomials were determined using a Nelder and Mead optimization algorithm, which maximizes a given generic function given a set of adjustable parameters. The optimized function in this case measured the degree of overlap in the two images using mutual information.

Mutual information is a concept borrowed from the field of information technology which determines probability that a set of pixels contain the same information, regardless of the independent values of the pixels. The mutual information of two images is related to the image entropy, H of the image defined by:

$$H = -\sum_{i=0}^{255} p_i \ln(p_i)$$

where p_i is the probability that a pixel within the image has an intensity of i, within the a range of 0 to 255. The joint entropy of two images, im1 and im2, measures the degree of correlation between the two images and is similar to the concept of the entropy of mixing in solutions, is given by:

$$H(im1,im2) = -\sum_{j=0}^{255}\sum_{i=0}^{255} p_{i,j} \ln(p_{i,j})$$

where pi,j is the probability that if im1 has an intensity of i then im2 has the probability of having intensity j. The mutual information, MI, between the two images is then given by:

$$MI(im1,im2) = H(im1) + H(im2) - H(im1,im2)$$

Thus, if the amount of shared information between the two images increases, the value of the MI will increase, regardless of the exact values of the features within the images. For further information on the use of mutual information for data alignment see [3].

The mutual information between the optical image and the “Band Contrast” image from the EBSD data was maximized, since both of these imaging modes provided strong contrast at the

location of the crack, as well as at the location of the grain boundaries. The initial guess for the modifications of the EBSD images was given by the ratio in pixel size of the two images, and a manual estimation of the translations for the first optical image/EBSD image pair. Subsequent initial guesses for the polynomial coefficients were given by the previous pair's solution.

Once the EBSD images were aligned to the optical images, they were combined into a single reference frame in the VTK framework for analysis.

Analysis

Initial analysis focused on the crystallographic nature of the opposing crack surfaces. Consequently, the crack was extracted from the optical portion of the 3D volume. Lines of EBSD data, spaced roughly every 5µm, were superimposed onto the extraction surface from the fully reconstructed volume. Next, a surface normal was estimated for each point on the crack surface in the volume reference frame. This was accomplished using in-house software, which was developed with VTK and designed to analyze 3D surfaces. The crystallographic normals were then calculated at points that contained EBSD data. These data, over 200,000 directions, are plotted in the [001] pole figure in Figure 4. There was a slight preference for <111> normal directions, which correspond to {111} planes along the crack surface. This begged the question as to whether there was a significant twin content in the crack path, which required analysis of the boundary planes themselves.

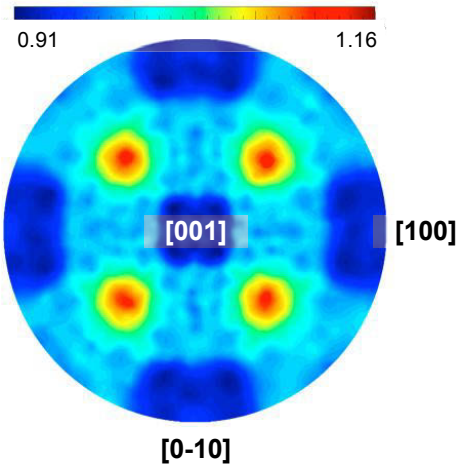

Figure 4 – [001] pole figure of surface normal directions. Scale is multiples of a random distribution.

To analyze the boundary planes that the crack followed, crystallographic normal directions from opposite sides of the crack were grouped in pairs and analyzed. Specifically, each point on one side of the crack was projected along its normal direction (in the volume reference frame) to the closest point on the opposite side, creating a pair. The two crystallographic surface planes of a pair and the axis/angle disorientation obtained from a pair's EBSD data were used to classify the crack boundary points into eight categories, which were color coded for visual representation:

- RED: Twin boundary = Σ3 disorientation with both boundary planes equal to {111}
- ORANGE: Σ3 boundary with only one {111} plane (1st plane)
- YELLOW: Σ3 boundary with only one {111} plane (2nd plane)
- MAGENTA: Σ3 boundary with no {111} plane on either side
- GREEN: Regular (non-Σ3) twist boundary with both boundary planes equal to {111}
- CYAN: Regular boundary with only one {111} plane
- BLUE: Regular boundary with no {111} plane on either side
- WHITE: Not a grain boundary

The tolerance for the Σ3disorientation was initially set to 5° for both the angle and axis. A 10° tolerance was also used for comparison. Results are shown graphically in Figure 5. The majority of planes that the crack followed were regular boundaries with either no {111} plane on either side of the crack (BLUE), or only one {111} plane (CYAN). The type with the next

highest frequency was a Σ3 boundary with no {111} plane on either side (MAGENTA). Virtually no twins (RED) or Σ3 boundaries with a single {111} plan (ORANGE, YELLOW) were present, although a small amount of regular twist boundaries (GREEN) were detected. The results suggest that the crack proceeded almost exclusively along regular boundaries.

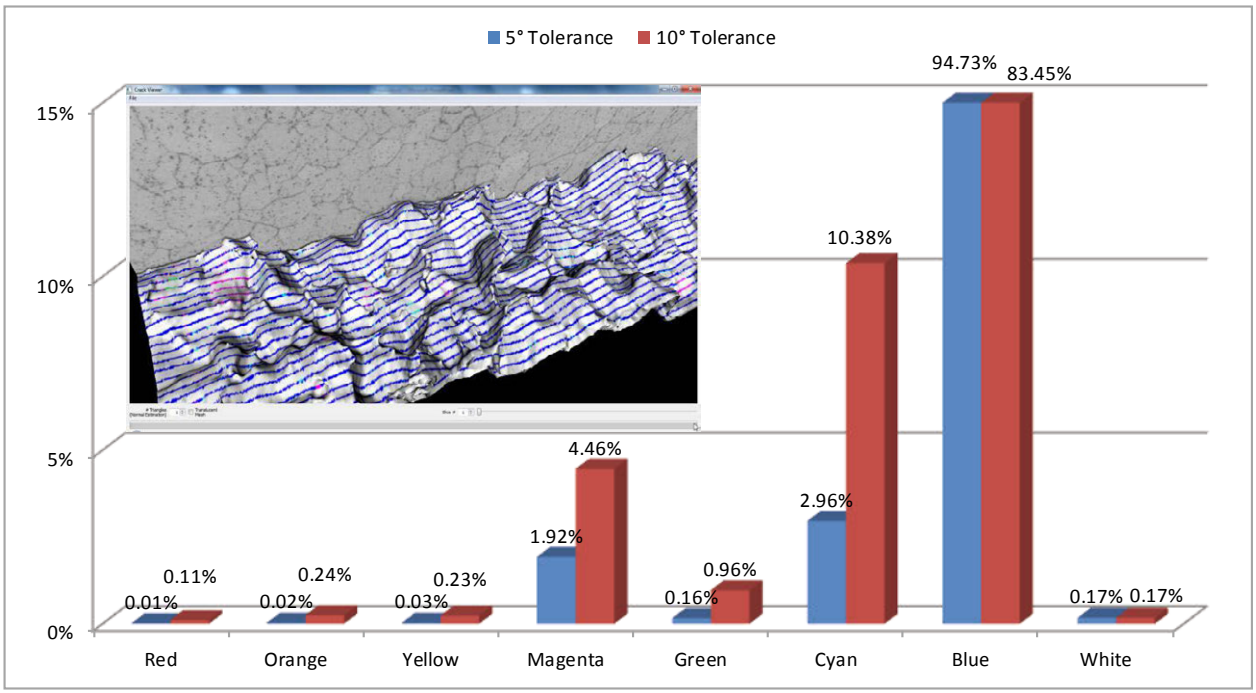

Figure 5 – Chart of boundary distribution. Inlaid image is a top-down view of the crack surface, with boundary coloring on the EBSD points and a single optical image orthogonal to the surface. See text for key.

Future Work

The authors plan to compare the data in Figures 4 and 5 to similar distributions obtained from the bulk portion of the 3D volume away from the crack surface. This will help determine whether the crack actively followed a regular boundary path or simply encountered the bulk distribution of boundary types along its trajectory. To accomplish this, segmentation of the grain boundaries in the optical data and incorporation of the twin boundaries from the EBSD data are both currently in progress.

References:

[1] Lewis, A.C. , Bingert, J.F., Rowenhorst, D.J., Gupta, A., Geltmacher, A.B., Spanos, G. "Two- and three-dimensional microstructural characterization of a super-austenitic stainless steel" Materials Science and Engineering A 418 (2006) 11–18.

[2] Nolze, G. "Image distortions in SEM and their influences on EBSD measurements." Ultramicroscopy 107 (2007) 172–183.

[3] Gulsoy, E. B., Simmons, J. P., De Graef, M. "Application of joint histogram and mutual information to registration and data fusion problems in serial sectioning microstructure studies." Scripta Materialia, 60 (2009) 381–384.